

RSC Advances



This is an *Accepted Manuscript*, which has been through the Royal Society of Chemistry peer review process and has been accepted for publication.

Accepted Manuscripts are published online shortly after acceptance, before technical editing, formatting and proof reading. Using this free service, authors can make their results available to the community, in citable form, before we publish the edited article. This *Accepted Manuscript* will be replaced by the edited, formatted and paginated article as soon as this is available.

You can find more information about *Accepted Manuscripts* in the [Information for Authors](#).

Please note that technical editing may introduce minor changes to the text and/or graphics, which may alter content. The journal's standard [Terms & Conditions](#) and the [Ethical guidelines](#) still apply. In no event shall the Royal Society of Chemistry be held responsible for any errors or omissions in this *Accepted Manuscript* or any consequences arising from the use of any information it contains.

Dynamics of chiral molecule in gaseous environments: validity of Magnus effect in microscale systems

Hong-Fei Chen, Wei-Rong Zhong[†]

(Siyuan laboratory, Guangzhou Key Laboratory of Vacuum Coating Technologies and New Energy Materials, Department of Physics, Jinan University, Guangzhou 510632, China)

Abstract

Dynamics and separation of chiral C60 are numerically investigated in gaseous environment with a linear velocity. We have found that the probability of location of center-of-mass coordinates of C60 on Y direction is affected by chirality of C60, angular velocity of C60, the temperature of gaseous environment, the pressure of gaseous environment and the species of the particle. When angular velocity is zero, the transport trajectory is close to the standard normal distribution on Y direction. For the clockwise C60, it has a higher probability to the positive Y-axis. However, the counterclockwise rotating C60 tends to approach the negative Y-axis. In addition, we also propose a mechanical mechanism in microscale systems about chiral separation. Our statistical results present a phenomenon that is different from the Magnus effect.

Keywords: Chiral Molecule; Fullerene; Magnus Effect; Molecular Dynamics Simulations;

1. Introduction

The Magnus effect is well-known for its influence on the flight path of a spinning ball. Seifert reviewed the application of Magnus effect devices and concepts in aeronautics⁽¹⁾. What is more, some researchers investigated the optical Magnus effect. Surface engineering in chemical and physical systems has been studied theoretically and experimentally⁽²⁾, except as the microparticles moving by Magnus effect. Above all, understanding the Magnus effect of the active particles in the microscopic world can provide insight into out-of-equilibrium phenomena associated with physical examples such as target material and C60. These phenomena may appear in several fields, e.g. coat material in polymer solar cells⁽³⁾, clean surface in material^{(4),(5),(6),(7)}, shield plating in workpiece and separate microparticles in chirality⁽⁸⁾. Compared with the passive

[†]Corresponding author. E-mail: wrzhong@hotmail.com

studies of active matter, microscopic particles moving in confined structures could exhibit peculiar behaviors, resulting for example in rotational cooperative particle motions distort the lattice and induce the free dislocations processes⁽⁹⁾. The presence of particles could destabilize the interface which, in turn, affected the behavior of particles at the interface⁽¹⁰⁾. Microparticles can be finely characterized or distinguished according to their distinct maximum synchronous velocity spectra⁽¹¹⁾.

Due to the high stability and the properties of well-characterized electron acceptor, C60 has attracted ongoing attention in many fields such as condensed matter physics and material science. Song *et al.*⁽¹²⁾ probe single quantum dot (QD) fluorescence spectroscopy distribution and its effect on the function (electron-transfer dynamics) in QD-C60 complexes. They found that in self-assembled QD nanostructures, the statistical distribution of the number of adsorbed partners can dominate the distributions of the averages and standard deviation of their interfacial dynamical properties. Some reviews had found the colloidal properties of fullerene C60 and multi-walled carbon nanotubes⁽¹³⁾. Richa and coworkers⁽¹⁴⁾ have studied nanocrystalline mixtures of Boron subphthalocyanine chloride and C60. Their device performance shows a strong dependence on active-layer donor–acceptor composition, and peak efficiency is realized at 80wt.% C60. These research strategies were mainly based on doping and physicochemical properties. However, in some situations, the mechanical properties of C60 are as important as them. For example, C60 can generate nanopores in graphene⁽¹⁵⁾, clean the surface and coating⁽¹⁶⁾. Therefore, a deeper understanding of dynamic properties of C60 is necessary for the advanced materials industries. Wang and James demonstrated correlation between mechanical wave and temperature variation at the early stage of collision⁽¹⁷⁾. The rebounding processes of C60-graphite surface collisions at different energies are found to exhibit similar dynamic behavior and the molecular center-of-mass motion can be regarded as moving in a quadratic harmonic potential⁽⁶⁾. Girifalco had researched the molecular properties of C60 in the gas and solid phases⁽¹⁸⁾. Moriarty had used anisotropic molecular manipulation to translate, rotate and remove C60 on Si (100)-2×1⁽¹⁹⁾. Liang and coworkers have investigated the effect of C60 molecular rotation on nanotribology experimentally⁽²⁰⁾. What is more, Aharonov-Carmi effect and energy shift of valency electrons in rotating C60 molecules had been studied⁽²¹⁾. These researches present an important issue about the dynamical behavior of rotating C60.

In this paper, we will numerically study the dynamics and collision of pure C60 in a channel with gaseous environments, and show our systematic molecular dynamics investigation on the movement formation induced by clusters through controlling the environmental temperature, the number of particles, the rotation angular velocity and the species of gas particles. To understand the process of particle collision in fluctuating environment more precisely, we use the method of simple statistical analyses to get its nature.

2. Model and methods

In the presence of an additional torque, the C60 tends to execute circular orbits called chiral C60. (e.g. chiral microswimmer)⁽⁸⁾. In this paper, we consider molecular dynamics simulations of collisions between C60 and gas particles and put them in a box with periodic boundary conditions. As is shown in Fig.1, the height (AE) is Y-direction, the width (AB) is X-direction and the length (BC) is Z-direction. v is the linear velocity of C60, which is perpendicular to the Y-direction. w is the angular velocity of C60, here the counterclockwise and clockwise direction in Y-Z plane are negative and positive direction, respectively.

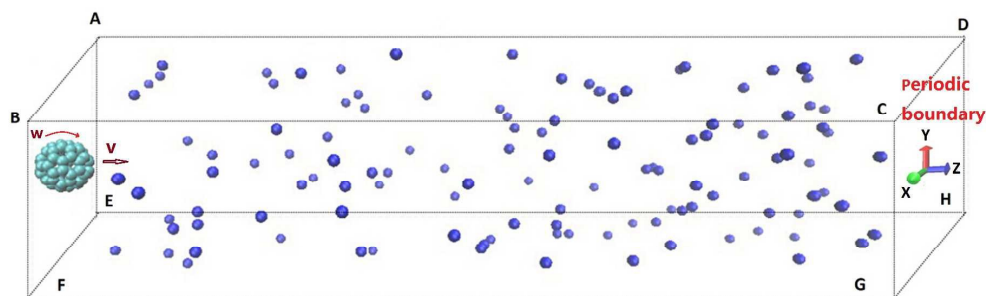


Fig.1 Scheme of separating device: two kind of chiral C60 moving in rare gas environment under periodic boundary conditions.

The big ball is C60 in the channel. The initial states of C60 include the position of center-of-mass coordinate (0, 0, 0). Its linear velocity v along Z-axis and its angular velocity w around X-axis. Periodic boundary conditions are imposed in the X, Y and Z directions. The light blue and dark blue balls denote carbon atoms and gas molecules, respectively.

We employ the classical molecular dynamics method based on the Tersoff-Brenner (TB) potentials of carbon-carbon (C-C) bonding interactions in C60 clusters.

$$V^{Tr}(r_{ij}) = f_c(r_{ij})[a_{ij}V^R(r_{ij}) - b_{ij}V^A(r_{ij})] \quad (1)$$

$$V^R(r_{ij}) = A_{ij}e^{-\lambda_{ij}r_{ij}}, V^A(r_{ij}) = B_{ij}e^{-\mu_{ij}r_{ij}} \quad (2)$$

where $V^R(r_{ij})$ represents the repulsive pair-wise interaction. $V^A(r_{ij})$ represents the attractive potential due to valence electrons. i and j refer to the atoms in C60. r_{ij} and μ_i, λ_{ij} is the distance and energy parameters of atoms and atoms in C60, respectively. For the sake of simplicity, we do not provide the parameters in detail (such as $A_{ij}, B_{ij}, a_{ij}, b_{ij}$), and all the parameters for Tersoff-Brenner potentials are given in Rafii-Tabar⁽²²⁾.

The Lennard-Jones (LJ) potentials^{(23),(24)} are used to expressed the van der Waals interactions of gas-gas and gas-carbon interactions and the form is

$$V_{LJ}(r_{ij}) = 4\epsilon \left[\left(\frac{\sigma}{r_{ij}} \right)^{12} - \left(\frac{\sigma}{r_{ij}} \right)^6 \right] . \quad (3)$$

The distance and energy parameters of this pair potential obtained with semi-empirical combining rules from the Lennard-Jones ϵ and σ parameters of the carbon atoms and the atoms in gas.

$$\sigma_{eg} = \frac{\sigma_{ee} + \sigma_{gg}}{2} , \quad (4)$$

$$\epsilon_{eg} = \sqrt{\epsilon_{ee}\epsilon_{gg}} , \quad (5)$$

where “e” and “g” refer to the atoms in rare gas and carbon atoms, respectively. while parameters of the atoms in C60 are given for some relevant systems in Table I.

TABLE I Parameters of Lenard-Jones potentials for different atoms.

Atom	$\sigma_{ee}(\text{\AA})$	$ \epsilon_{ee} (K)$
He-He ⁽²⁵⁾	2.560	10.9
Ne-Ne ⁽²⁵⁾	2.750	35.6
He-C ⁽²⁵⁾	2.980	19.3
Ne-C ⁽²⁵⁾	3.075	71.2

The dynamics of *ith* particle is described by the following Langevin equations

$$m \frac{d^2 r_i}{dt^2} = f_i(t) + F_i(t) \quad (6)$$

$$F_i(t) = -\frac{\partial V(r_i)}{\partial r_i}, f_i(t) = -\Gamma m v_i + \sqrt{2k_B m \Gamma T_0} \xi_i(t) \quad (7)$$

where m is the relative atomic mass of atoms i , r_i is the displacement of atoms, t is the time, $f_i(t)$ consists of two parts, one for viscous drag is $\Gamma m v_i$, and another for random forces is $\sqrt{2k_B m \Gamma T_0} \xi_i(t)$ since the randomness is an inherent property of molecular systems. $V(r_i)$ is

the potentials of atoms, which include TB and LJ potentials. v_i is the velocity of the atoms, Γ is the surface viscous coefficient when atom collision, the Gaussian white noise satisfies $\langle \zeta_i(t) \rangle = 0$, and $\langle \zeta_i(t) \zeta_j(s) \rangle = \delta_{ij} \delta(t-s)$. T_0 is the temperature of environment, k_B is the Boltzman constant. The random velocity of gas molecules depend on the distribution of Maxwell distribution. The time step is 0.55 fs, the simulation runs 3×10^4 time steps giving a total molecular dynamics time of 16.5 ps to obtain the center-of-mass coordinates of C60 in the Y-axis. k is normalized density of C60 falling Y-axis, which satisfies,

$$\int_{-\infty}^{+\infty} k dy = 1. \quad (8)$$

We define P as the rate of probability of C60 located on positive Y-axis (N_r) to that located on negative Y-axis (N_l). P can describe how much a chiral C60 tend to go to negative or positive Y-axis. The equations are defined as

$$P = \frac{N_l}{N_r} \quad (9)$$

where N_l and N_r are the frequency of the center-of-mass coordinate of C60 in negative and positive Y-axis when passing through the gas, respectively. If $P > 1$, it means C60 tends to deflect and fall to negative Y-axis, and vice versa. E is the standard error of P . which is defined as

$$\bar{P} = \frac{1}{n} \sum_{i=1}^n P_i, \quad E = \sqrt{\frac{1}{n-1} \sum_{i=1}^n (P_i - \bar{P})^2}, \quad (10)$$

where n is the number of simulations; P_i is the rate of probability of C60 located on Y-axis of data i , \bar{P} is the average of P_i .

3. Results and discussions

In this work, we propose two kinds of gaseous environment to test the validity of Magnus effect in microscale systems: (A) rotated C60 in the neon gaseous environment and (B) rotated C60 in the helium gaseous environment. Unless otherwise noted, our simulations are under the parameter sets: $AE=40 \text{ \AA}$, $AB=40 \text{ \AA}$, $BC=160 \text{ \AA}$ and $v=10 \text{ \AA ps}^{-1}$. Our statistics was on the basis of center-of-mass coordinates of C60. For the convenience of discussion, we focus on equimolar gaseous environment, where the number of the neon particles is equal to the number of the helium particles.

A. rotated C60 in the neon gaseous environment

In this section, we will systematically study the movement of rotated C60 in terms of w , T and N

in the presence of the neon gaseous environment.

At $T=350$ K and $N=288$, we do 2000 simulations repeatedly by using different w with $v=10$ Å ps⁻¹. Figure 2 shows the P as a function of the Y coordinate of C60. It is found that directed current occurs and the curves are almost the same for both clockwise and counterclockwise C60. When $w=0$, the value of P wandering around a straight dotted line $p=1$, it means that the distribution of C60 follows the standard normal distribution. When $w<0$, $|w|$ increases from zero to 15, the value of P is larger than one. It means that the distribution of counterclockwise C60 does not follow the standard normal distribution along $Y=0$, and more C60 particles move to the negative Y -axis. When $w>0$, the opposite results are observed and more C60 particles move to the positive Y -axis. In order to observe more conveniently, we employ the distribution of C60 at $w=-15, 0$ and 15 rad ps⁻¹. As is shown in the inset of Fig.2, the peak of the distribution of C60 have three positions. when $w=-15$ rad ps⁻¹, its peak locates on negative Y -axis. On the contrary, when $w=15$ rad ps⁻¹, its peak locates on positive Y -axis. Obviously, particles with different angular velocities can be separated in the flowing gaseous environment.

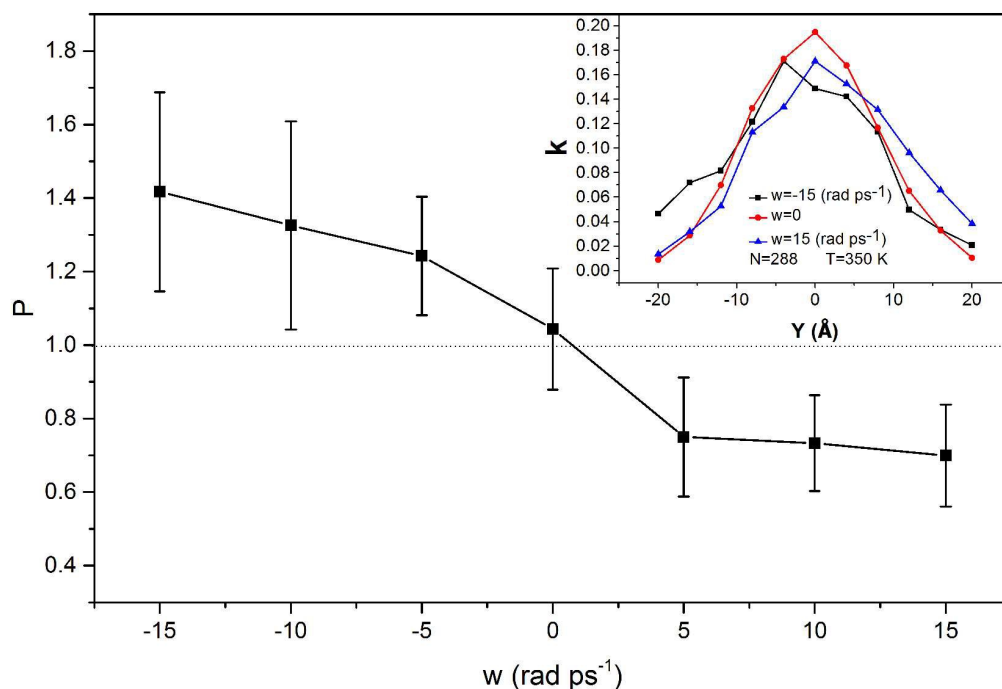


Fig.2 The rate P as a function of the rotation velocity w in neon gaseous environment. The inset is the normalized density k as a function of the Y -coordinate in neon gaseous environment with $w=-15, 0$ and 15 rad ps⁻¹. $T=350$ K and $N=288$.

In first section, we have observed that the distribution of rotated C60 depends on the angular

velocity in the gaseous environment. To analyze the separation of C60 considering rotate fluctuations, we can get its nature by using the same statistical analyses.

The probability of C60 located on the Y-axis as a function of the number of gas particle is shown in Fig.3. The peak of the distribution of C60 has three positions. For $N=128$, its probability curve has a peak located on negative Y-axis. For $N=200$ and $N=288$, the position of the peak of probability curve is the same as the former. Upon increasing N from 128 to 288, the ratio between the frequency of the center-of-mass coordinate of C60 in negative Y-axis and positive Y-axis decreases monotonically from 1.63 to 1.41 at $\omega=-15 \text{ rad ps}^{-1}$. It is suggested that counterclockwise C60 in the process of moving is more focused on the negative Y-axis with a relatively low pressure gaseous environment. In other word, with excessive gaseous particles, the separation of C60 will be hindered. Therefore, the counterclockwise particles will be separated to the negative Y-axis direction where the number of particles plays an important role.

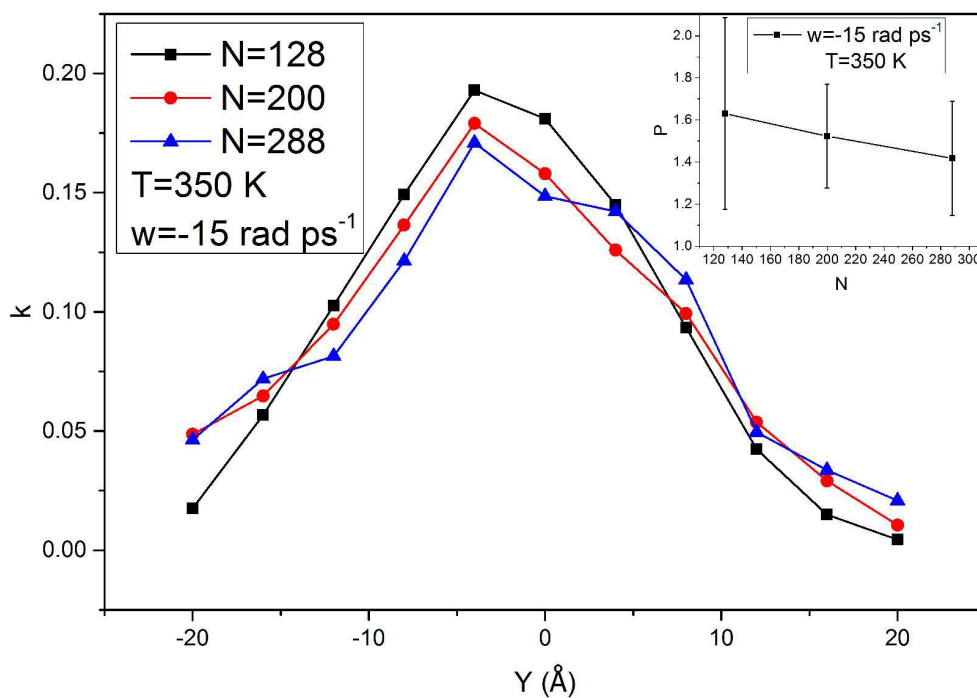


Fig.3 The rate k as a function of the Y-axis coordinates in neon gaseous environment. The inset is the rate P as a function of the number N in neon gaseous environment. $T=350 \text{ K}$ and $\omega=-15 \text{ rad ps}^{-1}$.

Fig.4 depicts the bar charts of the probability of C60 located on the Y-axis with the temperature fluctuations when $\omega=-15 \text{ rad ps}^{-1}$ and $N=288$. When the Y-coordinate varies from 0 to -20, it is found that the black bar charts are higher than other bar charts on the negative Y-axis. But for the

Y-coordinate from 0 to 20, the blue bar charts are higher than other bar charts on the positive Y-axis. Upon increasing T from 250 to 350 K, the ratio between the frequency of the center-of-mass coordinate of C60 in negative Y-axis and positive Y-axis decreases monotonically from 1.51 to 1.41. In a word, the effect of separation is the same. This is because the possible location of counterclockwise C60 is more inclined to the negative Y-axis. What is more, the rate P decreases monotonously with the temperature increasing. Therefore, the temperature is one of the factors that affect the particle separation.

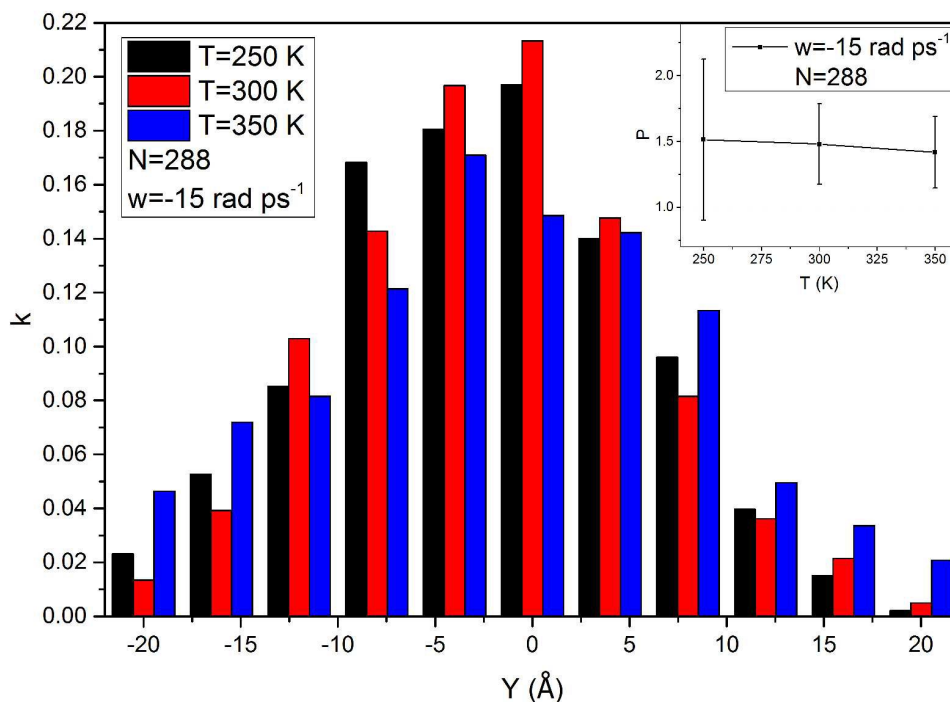


Fig.4. The bar chart of rate k on the Y-axis coordinates in neon gaseous environment. The inset is the rate P as a function of the temperature T in neon gaseous environment. $N=288$ and $w=-15$ rad ps^{-1} .

As is shown in Fig.2, we can note that the more w increases, the more friction increases, and then the angle of deflection becomes bigger. What is more, the collision frequency increases with the number of gaseous particle. Due to the collisions, w gradually decreases, and the effect of overall separation weakens. The probability of collision always increases with the temperature. When the restriction of collision become more obvious, the effect of separation abates. From Fig.4, we can find that the number of gaseous particle is enough, the effect of separation works well and is subdued with the increase of temperature.

B. rotated C60 in the helium gaseous environment

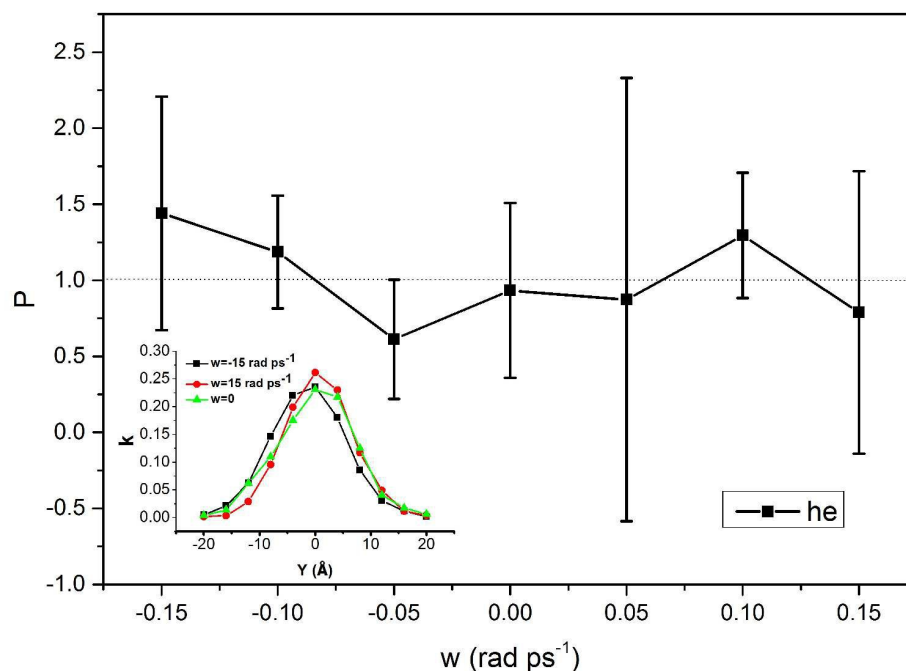


Fig.5 The rate P as a function of the rotation velocity w in helium gaseous environment. The inset is the normalized density k as a function of the Y -coordinate in neon gaseous environment at $w = -15, 0$ and 15 rad ps^{-1} . $T = 350$ K and $N = 288$.

The results of the helium gaseous environment are shown in Fig.5. It is found that the separation methods in the helium gaseous environment are not significant than neon gaseous environment. As the angular velocity increases, the rate P fluctuates. When $w = -15, 15$ and 0 rad ps^{-1} , the distinction of their curve was not obvious and tend to present the standard normal distribution. Compared to the neon gaseous environment, it is known to us that the mass and size of neon particle are bigger than the helium particle. From the above results, the efficiency of separation in gaseous environment is affected by changing the mass and the size of gaseous particles. Thus, it is possible to increase the efficiency of separation in gaseous environment experimentally.

C. Comparing rotated particles moving in gaseous environment in micro scale and macro scale

In macro scale, when the rotating angular velocity of rotating object has misalignment with its flight velocity, a lateral force will come into being on the vertical direction of phase plane of rotating angular velocity and the velocity. The phenomenon that the trajectories of objects deflects under the influence of transverse force is considered to be Magnus effect. For example, as is shown in Fig.6, the clockwise football will go down along negative Y -direction in gaseous environment.

On the contrary, in micro scale as shown in Fig.6, our studies suggested that the clockwise particles have a larger probability to go up along positive Y-direction in gaseous environment. We propose different mechanical mechanism should be considered.

The Magnus effect is determined by Bernoulli's law, which describes that the increase of fluid velocity will cause the decrease of the pressure, and the decrease of fluid velocity will cause the increase of the pressure. Thus the rotating object has the lateral pressure difference, and transverse force is formed.

In order to give the explanation of the mechanical mechanism of our statistical results, we plot the schematic diagram of the mechanical mechanism in Fig.6. As is shown in Fig.6, the collision between a rotating particle and a gaseous particle generates a applied force. Due to the existence of the angular velocity, the carbon atoms of area A begin to approach gaseous particles, thus producing an incremental van der Waals forces ΔF_1 . On the contrary, the carbon atoms of area B go away from gaseous particles, thus producing a deducing van der Waals force ΔF_2 . We ignore other areas due to the long distance ($>0.7\text{nm}$). According to nanotribology, C60 rotation does not provide an additional energy dissipation channel in the friction process and the interaction energy increases when shortening intermolecular distance⁽²⁰⁾. Hence, the difference between ΔF_1 and ΔF_2 can be regarded as a centripetal force in the movement of objects. According to the characteristic of van der Waals force, as displayed in the inset of Fig.6, $\Delta F_1 > \Delta F_2$, thus a join force (in positive Y-direction) will be produced, which leads to a change in the direction of flight under the interaction between a join force and a linear velocity. The results suggest that the cluster ion beam is a good tool for directional bombardment, doping, coating, membrane cleaning and chirality separation.

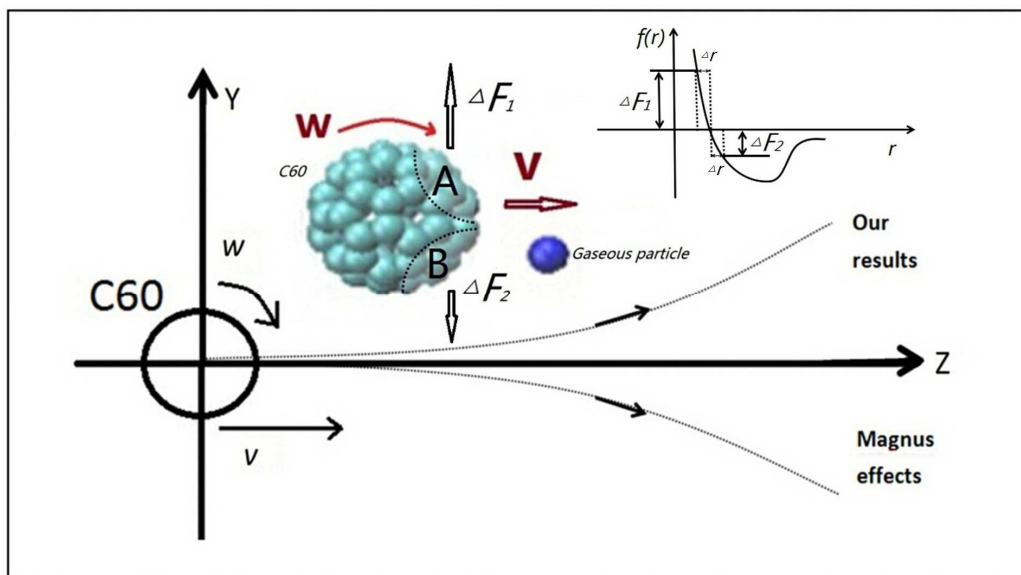


Fig.6 the Mechanical mechanism of Magnus effect and collision of particles. The inset is C60 molecule and gaseous particle and the van der Waals force of C60 molecule is as a function as intermolecular distance (r).

4. Concluding remarks

To conclude, we numerically studied the transport of different chiral C60 moving in steady gaseous environment of neon and helium. We have found that the probability of location of center-of-mass coordinates of C60 on Y direction is affected by the chirality of C60, angular velocity of C60, the temperature of gaseous environment, the pressure of gaseous environment and the species of the particle. The effect of the chirality comes about via the viscous drag. For the clockwise C60, it has a high probability to the positive Y-axis. On the contrary, it has a high probability to the negative Y-axis when the chirality of C60 is counterclockwise. The direction of the transport can be reversed by tuning the angular velocity. The angular velocity of C60 would significantly influence the probability of distribution by the energy of viscous drag. However, a relatively lower temperature of gaseous environment also can obviously reduce the probability of deflection due to the friction process. The pressure of gaseous environment plays an important role in the transfer process of C60. There exists an optimal value of the angular velocity and temperature at which the P has a direct proportion relationship with N . The mass and the size of gaseous particles will weaken the combined effect that the former factors above have that on the efficiency of separation in gaseous environment. We expect that our results can not only provide insight into the understanding of the mechanism of rotating C60 in gaseous environment, but also be applied potentially to the functionalization of C60, and the

production of C60-doping and C60-coating.

Acknowledgements

The authors would like to thank high performance computing platform of Jinan University and Siyuan clusters. This work was supported in part by the National Natural Science Foundation of China (Grant no. 11004082); the Natural Science Foundation of Guangdong Province, China (Grant no. 2014A030313367); and the Fundamental Research Funds for the Central Universities, JNU (Grant no. 11614341).

reference

1. Seifert J. A review of the Magnus effect in aeronautics. *Progress in Aerospace Sciences*. 2012;55(5):17-45.
2. K.Yu. Bliokh, YPB. Topological spin transport of photons: the optical Magnus effect and Berry phase. *Physics Letters A*. 2004;333(3-4):181-6.
3. D. Wynands, ML, M. Riede, M. Pfeiffer, P. Baeuerle, R. Rentenberger, P. Denner, K. Leo. Correlation between morphology and performance of low bandgap oligothiophene:C60 mixed heterojunctions in organic solar cells. *Journal of Applied Physics*. 2010;107(1):014517.
4. Inui N MK, Moritani K. Actuation of a suspended nano-graphene sheet by impact with an argon cluster. *Nanotechnology*. 2008 Dec 17;19(50):4887-92. PubMed PMID: 19942769.
5. Takazumi K, SO, Yoshiyuki M, Atsushi O. Carbon three-dimensional architecture formed by intersectional collision of graphene patches. *Physical Review B*. 2005;72(3):035428.
6. Z. Y. Pan, Z. Y. Man, YKH, J. Xie and Y. Yue. Energy dependence of C60 – graphite surface collisions. *JOURNAL OF APPLIED PHYSICS*. 1998;83(9):4963-7.
7. Zuo G H, ZX, Huang Q, Fang H P, Zhou R H. Adsorption of Villin Headpiece onto Graphene, Carbon Nanotube, and C60: Effect of Contacting Surface Curvatures on Binding Affinity. *The Journal of Physical Chemistry C*. 2011;115(47):23323-8.
8. Ai Bao-quan, HY-f, Zhong Wei-rong. Chirality separation of mixed chiral microswimmers in a periodic channel. *Soft Matter*. 2015;11(19):3852-9.
9. Chiang C H, LI. Cooperative Particle Motions and Dynamical Behaviors of Free Dislocations in Strongly Coupled Quasi-2D Dusty Plasma. *Physical review letters*. 1996;77(4):647-50.
10. D. SHANGGUAN, SA, D.M. STEFANESCU. An analytical model for the interaction between an insoluble particle and an advancing solid_liquid interface. *METALLURGICAL TRANSACTIONS A*. 1992;23A(2):669-80.
11. Xiaolu Zhu, HY, Zhonghua Ni. Frequency-dependent behaviors of individual microscopic particles in an optically induced dielectrophoresis device. *Biomicrofluidics*. 2010;4(1):13202. PubMed PMID: 20644665. Pubmed Central PMCID: 2905262.
12. Nianhui Song, HZ, Shengye Jin, Wei Zhan, Tianquan Lian. Poisson-Distributed Electron-Transfer Dynamics from Single Quantum Dots to C60 Molecules. *ACS NANO*. 2011;5(1):613-21.
13. Kai Loon Chen, BS, William P. Ball, D. Howard Fairbrother. Assessing the colloidal properties of engineered nanoparticles in water: case studies from fullerene C60nanoparticles and carbon nanotubes. *Environmental Chemistry*. 2010;7(1):10-27.
14. Richa Pandey, AAG, K. Andre Mkhoyan, and Russell J. Holmes. Efficient Organic Photovoltaic Cells Based on Nanocrystalline Mixtures of Boron Subphthalocyanine Chloride and C60. *Advanced Functional Materials*. 2012;22(3):617-24.

15. Xu Zhi-Cheng, ZW-R. Probability of self-healing in damaged graphene bombarded by fullerene. *Applied Physics Letters*. 2014;104(26):261907.
16. Akshay Rao, MWB, Wilson, Justin M. Hodgkiss. Exciton Fission and Charge Generation via Triplet Excitons in Pentacene/C60 Bilayers. *J AM CHEM SOC*. 2010;132(36):12698-703.
17. Wang X Q, LJD. Heat Wave Driven by Nanoscale Mechanical Impact between C60 and Graphene. *Journal of Nanomechanics and Micromechanics*. 2012;2(2):23-7.
18. Girifalco LA. Molecular Properties of C60 in the Gas and Solid Phases. *J Phys Chem*. 1992;96(2):858-61.
19. P. Moriarty, YRM, M.D. Upward, P.H. Beton. Translation, rotation and removal of C 60 on Si (100)-2× 1 using anisotropic molecular manipulation. *Surface Science*. 1998;407(8A):27-35. Epub 35.
20. Liang QT, O. K. Xu, Y. Li, H. Xiao, X. Effect of C60 molecular rotation on nanotribology. *Physical review letters*. 2003 Apr 11;90(14):146102. PubMed PMID: 12731932.
21. Shen Jian-Qi, HS-L. Aharonov-Carmi effect and energy shift of valency electrons in rotating C60 molecules. *European Physical Journal D*. 2005;33(1):35-8.
22. H R-T. *Computational Physics of Carbon Nanotubes*. New York: Cambridge University Press; 2008.
23. W BD. Empirical potential for hydrocarbons for use in simulating the chemical vapor deposition of diamond films. *Physical Review B*. 1990;42(15):9458-71.
24. L. A. Girifalco, MH, Roland S. Lee. Carbon nanotubes, buckyballs, ropes, and a universal graphitic potential. *PHYSICAL REVIEW B*. 2000;62(19):13104-10.
25. G Stan, MJB. Uptake of gases in bundles of carbon nanotubes. *PHYSICAL REVIEW B*. 2000;62(3):2173-80.

Abstract

Dynamics and separation of chiral C60 are numerically investigated in gaseous environment with a linear velocity. We have found that the probability of location of center-of-mass coordinates of C60 on Y direction was affected by chiral of C60, angular velocity of C60, temperature of the gaseous environment, pressure of the gaseous environment and the species of the particle. When angular velocity is zero, the transport trajectory are close to the standard normal distribution on Y direction. For the clockwise C60, it have high probability to the positive Y-axis. However, the counterclockwise rotating C60 tends to the negative Y-axis. In addition, as shown in Fig.A, we also proposed a mechanics mechanism in microscale systems about chiral separation. Our statistical results present a phenomenon that is different from the Magnus effect.

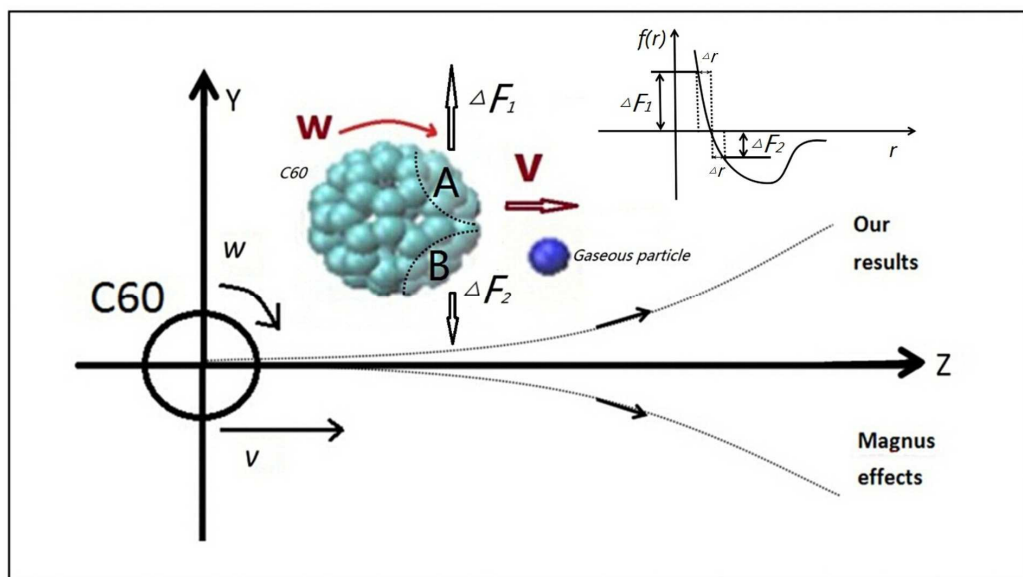


Fig.6 the Mechanics mechanism of Magnus effect and collision of particles. The inset is C60 molecule and gaseous particle and the van der Waals force of C60 molecule as a function as intermolecular distance (r).